https://doi.org/10.2352/ISSN.2470-1173.2018.15.COIMG-273


# Warping-based Motion Artefact Compensation for Multi-Line Scan Light Field Imaging

***Nicole Brosch; Svorad Štolc; Doris Antensteiner; AIT Austrian Institute of Technology; Vienna, Austria***

## Abstract

*This work focuses on the compensation of motion artefacts that may occur during a line scan acquisition and can be detected with our multi-line scan imaging system [10]. These artefacts are caused by fluctuations of the transport velocity that are not correctly reflected by the camera trigger, and are especially visible at high magnifications. We reduce such artefacts by analyzing the light field acquired with our system. Specifically, we use a variational formulation to design a warping function, such that lines that are acquired too early or too late are stretched or squeezed appropriately. To this end, we exploit the information comprised in the light field, i.e., control the estimation of the warping function by comparing light field views and enforce uniform spacing between line acquisitions. The proposed approach enables our system to perform the multi-line scan light field imaging at virtually any magnification independent from the transport and trigger quality. We demonstrate the capabilities of our approach for various objects by comparing 3D reconstructions from unprocessed acquisitions and our corrected acquisitions. Our approach significantly reduces artefacts in light fields and in 3D reconstructions that are generated from them.*

## Introduction

Line scan imaging enables high-speed and high-resolution image acquisition of continuously moving objects and, therefore, is a popular choice when performing industrial quality inspection tasks [3, 7]. However, when capturing moving objects *motion artefacts* may arise when the movement (i.e. the transport velocity) of the object is not perfectly synchronized with the line scan camera [3, 10, 12]. This becomes a serious issue especially when line scanning is performed at high magnifications. If such motion artefacts occur, the acquired line scan data would be subject to spatial distortions that can hinder the visual quality inspection.

This paper focuses on the compensation of such motion artefacts or synchronization artefacts. While in conventional line scanning (i.e., single line) such artefacts are not distinguishable from the correct signal, they become visible in light fields acquired with a multi-line scan system such as ours [1, 10]. Similar to conventional systems, our multi-line system acquires objects in motion, i.e., they are placed on a linear transport stage that is (loosely) synchronized with a camera. The transport stage moves with known direction past the multi-line camera (Figure 1, left). Each line of the system's camera captures the object under a different direction and, over time, contributes to a different view of the object. These views compose a linear light field [2], which is stored in an *epipolar plane image* (EPI) stack (Figure 1, right). As mentioned in [10], the synchronization between line acquisitions and the transport is crucial. If the linear transport stage is loosely

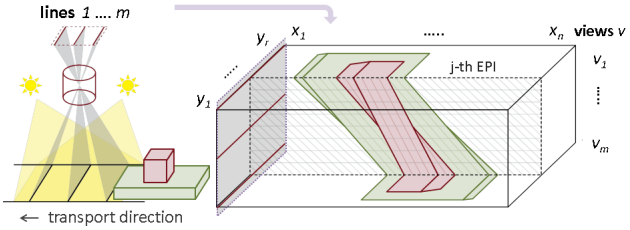


***Figure 1.*** *Illustration of our multi-line scan image acquisition setup [10] (left). At each space instance a set of $m$ lines is captured, then the object is moved by a linear transport stage. Multi-line frames with position index $x_i$ are acquired simultaneously. Each camera line captures the object under a different viewing angle and, over the time, contributes to a different view of the object. Each view $v_k$, consist of line acquisitions with indices $x_i$. The views compose a linear light field, which is stored in an epipolar plane image (EPI) stack $V_{y_j}(x_i, v_k)$ [2] (right). Figure taken from [10].*

synchronized with the camera or if there is some trigger jitter in place, the system acquires sets of multiple lines at non-uniform space instances. In this case, the captured views can contain motion artefacts, i.e., incorrect resolution in the transport direction due to squeezed or stretched lines. When considering a slice through all captured views, i.e., the EPI domain of the light field (Figure 1, $j$-th EPI), the motion artefacts are visible as deformed non-linear curves of corresponding object points (Figure 3, a) instead of lines (Figure 3, b). Consequently, the motion artefacts may also distort otherwise quite accurate 3D reconstructions (Figure 2, a) that can be generated from the light field. At high magnifications, this can be the case even when high-end hardware components are used. Thus, motion artefacts put a strong limit on magnifications that can be used a multi-line scan system.

Our proposed motion artefact compensation approach significantly reduces the mentioned artefacts in the light field views and the 3D reconstructions that are generated from them. We achieve this by leveraging the rich pixel information provided in the light field that was acquired with our system [10]. Our proposed approach is based on a warping function that is computed by a variational optimization procedure (e.g., [4, 8]). The true transport positions of the line acquisitions in the light field are recovered by constraining them according to the information obtained by comparing multiple views and enforcing uniform spacing between its line acquisitions. Subsequently, the undistorted views are computed by warping the distorted views according to the determined true positions of the line acquisitions. Hence, the proposed approach allows multi-line scan light field imaging at virtually any magnification with correct resolution in the transport direction (i.e., without squeezed or stretched pixels). It further enables pre-

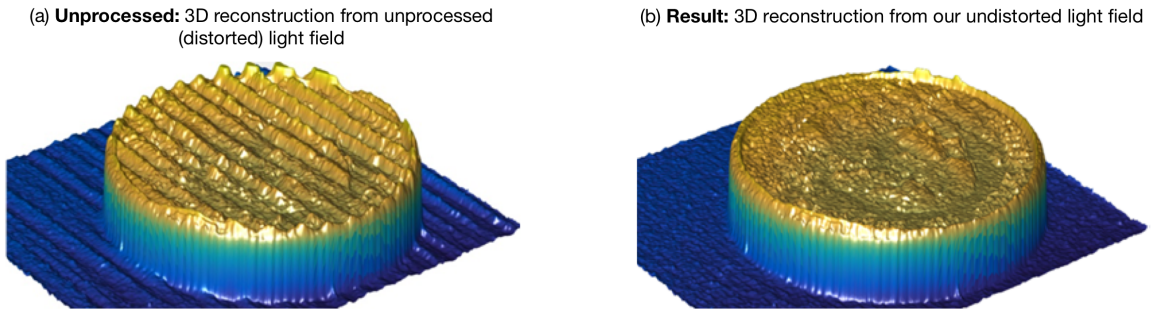


***Figure 2.*** *Visual comparison of 3D reconstructions generated from unprocessed (a) and our undistorted (b) light field acquisition of a coin with [10]. The motion artefacts in the 3D reconstruction from the unprocessed light field (i.e., ripples in (a)) are significantly reduced in the 3D reconstruction from our undistorted light field (b). Note that for this example we used a free running camera (no synchronization via camera trigger) in order to increase the visibility of motion artefacts.*

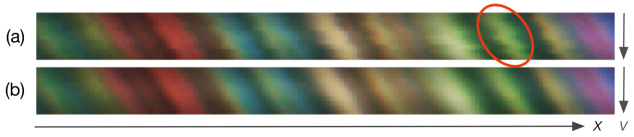


***Figure 3.*** *Visual comparison of unprocessed (a) and our corrected (b) EPI from an acquisition with our multi-line scan system. The motion artefacts in the unprocessed distorted EPI are visible as deformed non-linear curves which contain ripples (e.g. the ones highlighted red in (a)). These artefacts are significantly reduced in our undistorted EPI.*

cise 3D sensing using the multi-line scan light field approach not only at high magnifications but also in any use case where transport cannot be controlled with high precision.

The standard solution to motion artefacts or synchronization artefacts in line scan imaging, is to use high-end hardware components, such as high-precision transport stages and motion sensors [3]. However, we have observed that despite such hardware, acquisitions might sill suffer from motion artefacts. While the importance of compensating for motion artefacts was already stressed by existing line scan imaging approaches (e.g., [3, 10, 12]), to the best of our knowledge, a warping-based motion artefact compensation approach for improving integrity of multi-line scan light field data did not exist before.

More related research efforts can be found outside the realm of line scanning (e.g., in [4, 5, 6, 8, 11]. In some similarity to our work, in [11] motion is compensated in context of a 3D scanning system. It reconstructs the scene using a stereo phase shift method, which requires the successive projection of structured light patterns on a dynamic scene, e.g. on a moving object. Since the object's motion affects the projected pattern, the 3D reconstruction suffers from motion artefacts, i.e. an additional motion-caused phase shift that has to be distinguished from structure-caused one. Based on the assumption of uniform object motion, the motion-caused phase shift was estimated in a Taylor series and explicitly considered in their 3D reconstruction. In [5] a light field representation is generated from a video that was captured with a horizontal-moving smartphone camera. To this end, a subset of equally spaced frames is identified according to an additionally recorded control pattern, i.e., by selecting them according to certain control points. In [6] spectral inferograms that are affected by trigger jitter are aligned to reference inferograms in order to improve the precision of phase measurement from swept source optical coherence tomography systems. For this purpose internal reflections in such a system were used as reference for the alignment. In some relation to our work, visual media retargeting techniques determine new pixel positions (and thus, squeeze / stretch pixels) to adapt the given media to a different resolution and aspect ratio. These techniques are typically based on variational formulations, which are similar to ours, to determine the new pixel positions. Unlike to our approach, these variational formulations focus on content-aware scaling according to a saliency measure (e.g., [8]). Another related approach often used in stereo vision is the bundle adjustment [4]. This method seeks to optimize a subset of camera model parameters (e.g., camera position and rotation) along with 3D coordinates of the scene in one joint process in order to get the most consistent 3D reconstruction. Our approach can be seen as a simplified version of bundle adjustment tailored to the line scan scenario that attempts to find the most plausible sequence of virtual camera positions along the transport that minimize artifacts observed in the acquired light field data.

This paper is organized as follows: The next section describes two versions of the proposed motion artefact compensation approach. Then we compare these versions on light fields acquired with our multi-line scan system in order to evaluate the proposed artefact compensation algorithms. Since motion artefacts are especially visible in 3D data, we show disparity maps in the experimental result section. Finally, we conclude the paper with the discussion about obtained results.

## Algorithm Description

Given a light field that is stored in an EPI stack $V \in \mathbb{R}^{n\times m\times r}$ (e.g., Figure 1), where $V(x_i, v_k, y_j)$ with $1 \leq i \leq n$, $1 \leq k \leq m$ and $1 \leq j \leq r$, our motion artefact compensation problem can be described as follows. If the transport velocity is not perfectly synchronized with the multi-line scan camera (e.g., loose trigger), the gap between successive acquired lines is not constant. This leads to axis-aligned spatial distortions of the assumed integer indices $x_i$, i.e., squeezed and stretched pixels and, thus, true sub-pixel indices $\tilde{x}_i$. To compensate for such motion artefacts, i.e., the discrepancy between $x_i$ and $\tilde{x}_i$, we first determine $\tilde{x}_i$ in a variational formulation, and then unwarp (i.e., stretch / squeeze) pixels in $V$ accordingly. In this manner, we want to generate a new EPI stack, with uniform gaps between its position indices $\tilde{x}_i$.

Our proposed approach is based on the observation that motion artefacts become visible in 3D reconstructions (e.g., Figure 2, a), such as disparity maps that are generated from light fields acquired with our multi-line scan system [10]. In these light fields the same object point is captured in different views at different indices $x_i$, whereas the disparity is defined as the difference of these indices. In this context, an object point and an entire multi-line frame associated with $x_i$ that was performed too early or too late, causes a smaller or larger disparity than expected. In order to determine a true index $\tilde{x}_i$, i.e., a new position label $\tilde{x}_i$ for the i-th multi-line frame that was originally associated with $x_i$, we use previously estimated disparities to locate corresponding multi-line frames in different views. We then adjust the position of the i-th mutli-line frame from $x_i$ to $\tilde{x}_i$ by keeping the positions of its found corresponding frames fixed and in a manner that compensates for motion artefacts. More precisely, to find the true sub-pixel indices $\tilde{x}_i$, that correspond to each observed index $x_i$, we formulate an energy function consisting of a *disparity* term $E_d$, incorporating the observation mentioned above, an *identity* term $E_x$, which enforces a monotonous and stable solution, and a *smoothness* term $E_s$ that preserves a smooth and consistent indexing:

$$\min_{\tilde{x}} \frac{1}{2}\|E_d(\tilde{x})\|^2 + \frac{\lambda_1}{2}\|E_x(\tilde{x})\|^2 + \frac{\lambda_2}{2}\|E_s(\tilde{x})\|^2. \tag{1}$$

Here, $\lambda_1$ and $\lambda_2$ are used to balance the energy terms. The L-2 penalization of the disparity term $E_d$ can be generalized and exchanged with an L-1 penalization to better handle sparse errors of the disparity estimates. Below, we will discuss each energy term in more detail. For the disparity term we introduce two versions.

**Version 1: Constant background disparity** (Figure 4, a). Disparities that are computed in a flat fronto-parallel background stripe of an ideal light field with uniformly spaced $x_i$ should be constant[1]. For distorted light fields this is not the case (e.g., Figure 2, a; ripples in flat background regions), because the observed distorted indices $x_i$ directly affect disparities that are computed from them. By assuming a constant disparity in a background stripe, we can construct a disparity term $E_d$ of a minimization problem that ties together the searched true indices $\tilde{x}_i$ and estimated disparities. Hence, the disparity term can be written as:

$$E_d(\tilde{x}) = D\tilde{x} - \dot{d}, \tag{2}$$

where $\dot{d} \in \mathbb{R}$ is the mean disparity between any two consecutive views $v_k$ and $v_{k+1}$ over all background pixels and $D \in \mathbb{R}^{n\times n}$ is a special linear difference operator constructed from disparities $d_i$. As the result we get the following set of linear equations that constitute the first part of the least-squares problem defined in Eq. (1):

$$\begin{aligned}(\tilde{x}_{i+\lfloor d_i \rfloor}(1 - d_i + \lfloor d_i \rfloor) + \\ \tilde{x}_{i+\lceil d_i \rceil}(d_i - \lfloor d_i \rfloor) - \tilde{x}_i) - \dot{d} \approx 0, \\ \forall i \in \{1,...,n\}.\end{aligned} \tag{3}$$

More precisely, we first estimate sub-pixel disparities between two views $v_k$ and $v_{k+1}$ in a cropped background stripe, e.g. using the OpenCV 3.2 [9] stereo matcher. Then we determine a mean disparity $d_i$ in each position index $x_i$ and the mean disparity $\dot{d}$ over the entire cropped background. These parameters are then used in Eq. (3).
Obviously, this fomulation is not practicable when acquiring non-flat objects. In this case, the EPI stack might not contain a flat background region spanning along the entire acquisition that is a prerequisite of this version of the proposed algorithm. In the next section we provide an alternative formulation of the disparity term $E_d$, that makes no assumption about the scene's geometry.

**Version 2: Balanced foreward & backward disparities** (Figure 4, b). When considering an ideal light field with uniformly spaced $x_i$, the disparities between same structures in neighboring views should be balanced. Thus, we estimate forward disparities between views $v_k$ and $v_{k+1}$, and backward disparities between views $v_k$ and $v_{k-1}$. Analogue to the first version of our disparity term, we determine the mean forward disparity $d_{k,i}$ and the mean backward disparity $\bar{d}_{k,i}$ in each index $x_i$. In an ideal light field, the mean forward disparity $d_{k,i}$, computed between $v_k$ and $v_{k+1}$, and the mean backward disparity $\bar{d}_{k,i}$, computed between $v_k$ and $v_{k-1}$, for an index $x_i$ should be consistent, i.e., should cancel each other out. Thus, given $d_{k,i}$ and $\bar{d}_{k,i}$ for each position index $x_i$, we can infer the true indicies $\tilde{x}_i$ with our second version of our disparity term:

$$E_d(\tilde{x}) = D'\tilde{x}, \tag{4}$$

where for each position index $x_i$ for which both forward and backward disparities exist, we form one line in matrix $D' \in \mathbb{R}^{n\times n}$. The corresponding set of linear equations for the least squares problem in Eq. (3) for any give view $v_k$ $k \in \{2,...,m-1\}$ are as follows:

$$\begin{aligned}-2\tilde{x}_i + \tilde{x}_{i+\lfloor d_{k,i} \rfloor}(1 - d_{k,i} + \lfloor d_{k,i} \rfloor) \quad + \\ \tilde{x}_{i+\lceil d_{k,i} \rceil}(d_{k,i} - \lfloor d_{k,i} \rfloor) \quad + \\ \tilde{x}_{i+\lfloor \bar{d}_{k,i} \rfloor}(1 - \bar{d}_{k,i} + \lfloor \bar{d}_{k,i} \rfloor) \quad + \\ \tilde{x}_{i+\lceil \bar{d}_{k,i} \rceil}(\bar{d}_{k,i} - \lfloor \bar{d}_{k,i} \rfloor) \quad \approx \quad 0, \\ \forall i \in \{1,...,n\}.\end{aligned} \tag{5}$$

Our second disparity term therefore chooses $\tilde{x}_i$ in such a way that the obtained solution minimizes curvature of EPI-lines for the given triplet of views $v_{k-1}$, $v_k$ and $v_{k+1}$. Note that, since the $m$ lines of the multi-line camera simultaneously capture different parts of the object, the transport artefact at $x_i$ is the same in all these views but overlaid with different object parts. Thus, the recovered true index $\tilde{x}_i$ can be computed from all views $v_k$. In contrast to the first version of our disparity term, in this second version the estimation of the sub-pixel disparities $d_{k,i}$ and $\bar{d}_{k,i}$ in each position index $x_i$ are not restricted to a background stripe. The disparities can be computed over the entire view or a copped stripe (i.e., fixed $y_j$ values) that may contain a non-flat 3D object.

**Identity term.** To stabilize the solution and preserve its monotonicity, we assume that the actual movement is similar to the assumed ideal movement of the transport stage:

$$E_x(\tilde{x}) = x - \tilde{x}. \tag{6}$$

[1] We assume that the camera sensor is perfectly aligned with the transport and an ideal lens is used.

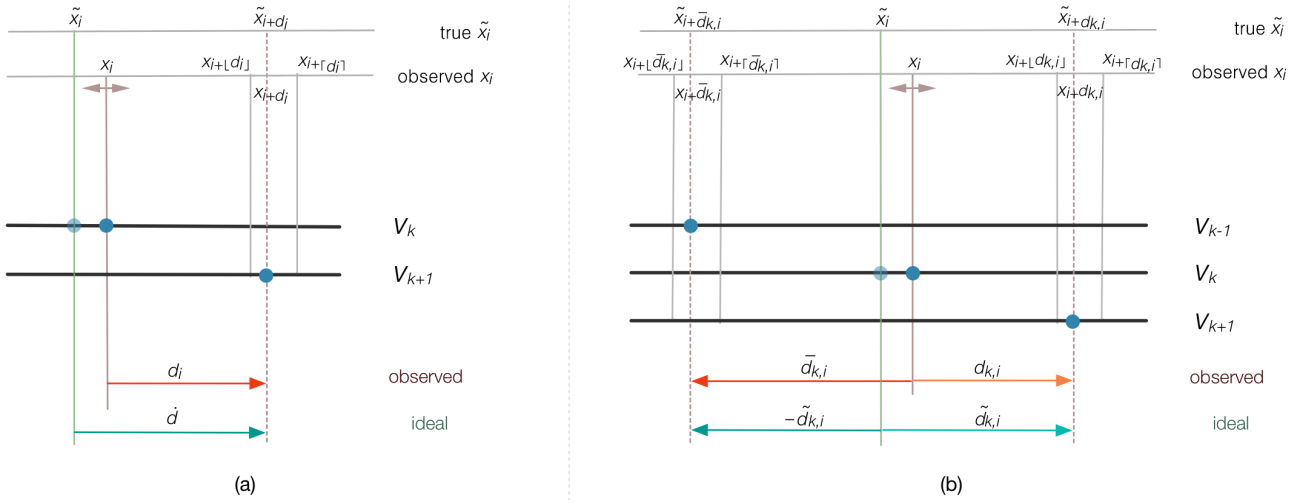


***Figure 4.*** *Illustration of the first (a) and second (b) version of our disparity term. Both versions are based on previously estimated disparities ($d_i$), which relate corresponding object points (dark blue points) in different views ($v_{k-1}$, $v_k$, $v_{k+1}$). In presence of transport issues, data points are acquired too early / late (light versus dark blue point in $v_k$) and the observed index $x_i$ of a multi-line frame differs from its true index $\tilde{x}_i$. (a) Version 1: The disparities in a flat fronto-paralell background stripe of an ideal EPI stack should not vary (light blue point). Thus, true indices $\tilde{x}_i$ can be determined according estimated disparities $d_i$ (red arrow) and the mean background disparity $\dot{d}$ (green arrow), which were both assessed in a background stripe of the acquired EPI stack. (b) Version 2: In an ideal EPI stack fore- and backward disparities are balanced ($\tilde{d}_{k,i}$, green arrows). In a distorted EPI stack with observed $x_i$ and disparities $\bar{d}_{k,i}$ and $d_{k,i}$ (red and orange arrow) this is not the case. However, for $x_i$, a true $\tilde{x}_i$ can be determined by enforcing this balance between its found corresponding points ($\tilde{x}_{i+\bar{d}_{k,i}}$ and $\tilde{x}_{i+d_{k,i}}$).*

Hence in Eq. (3), we also solve the set of equation:

$$x_i - \tilde{x}_i \approx 0, \quad \forall i \in \{1,...,n\}. \tag{7}$$

**Smoothness term.** In order to ensure smoothness of the solution $\tilde{x}_i$, we penalize abrupt changes between neighboring reconstructed position indices by

$$E_s(\tilde{x}) = \Delta\tilde{x}, \tag{8}$$

where $\Delta$ denotes the Laplacian operator, which is implemented in form of a convolution filter with the kernel $[1,-2,1]$. Thus, we form another set of linear equations as follows:

$$-2\tilde{x}_i + \tilde{x}_{i-1} + \tilde{x}_{i+1} \approx 0, \quad \forall i \in \{1,...,n\}. \tag{9}$$

We express the energy term in Eq. (1) as an overdetermined linear system of equations described in Eqs. (3) or (5), and (7) and (9), which can be solved only approximately using a least squares solver based, e.g., on a standard conjugate gradient method. Once the true indices $\tilde{x}_i$ are computed, the undistorted views are computed by warping the distorted views according to the determined true positions of the acquired multi-line frames. This results in a local stretching or squeezing of the EPI stack compensates for motion artefacts.

## Experimental Results

We perform our experiments on $2320 \times 4212 \times 11$ EPI stacks that were obtained with our multi-line scan system [10] with an optical resolution of 13.7 $\mu$m in the focal plane. In this configuration, our unoptimized MATLAB implementation requires 0.20 seconds to recover $\tilde{x}_i$ in a system of equations that consist of 12636 equations and is based on the first disparity term. When using the second disparity term, our system of equations contains 46332 equations and our algorithm requires 0.22 seconds to recover $\tilde{x}_i$. In order to increase the visibility of motion artefacts in our acquisitions, our experiments are also performed on a *free running dataset*, i.e., *Note1*, *Note2*, *PCB1*, *PCB2*, *Coin1* and *Coin2*. For these acquisitions, we used a free running camera without synchronization with the transport stage via trigger. Our experiments consider both versions of our disparity term. Disparities are estimated in different regions of the unprocessed EPI stacks, i.e., in a (assumed flat) background stripe and in a foreground stripe that might contain a 3D non-flat object.

Since motion artefacts are especially visible in the 3D data (e.g., ripples in Figure 2, a; Figure 5, top), such as disparity maps, the experimental results of our approach will focus on them. In Table 1 and Figure 5, we compare disparity maps that were generated from the (unprocessed) distorted and from our undistorted EPI stacks. In particular, Table 1 lists the standard derivation of disparities within a (assumed flat) background region. Since the disparity maps in such a region should be constant, the standard deviation can be used as a quality measure, where low values indicate less artefacts than larger ones. It can be seen that the majority of disparity maps which were generated from our corrected EPI stacks exhibit lower standard variations than those generated from the distorted EPI stacks. The motion artefact compensation with the first version of our disparity term and background disparities (V1 BG) and with the second version of our disparity term (V2 BG and V2 FG) reduced the average variation by a factor of 2.7. This indicates a significant reduction of the motion artefacts in our test data. As expected, the first version of our disparity term fails when its underlying assumption is violated (Table 1, V1 FG). When assuming a constant disparity within a foreground stripe that may contain objects (hence varying disparities), the dis-

**Table 1. Quantitative evaluation of the proposed motion artefact compensation approach. The table lists the standard deviation of pixel disparities in a flat background region. Our approach is evaluated in two versions, i.e., with the first (V1) and the second (V2) version of our disparity term, and when applying them with disparities that were estimated in a background (BG) and foreground (FG) stripe of the distorted EPI stack.**

| Data set | Distorted | V1 BG | V1 FG | V2 BG | V2 FG |
|---|---|---|---|---|---|
| free running camera | | | | | |
| *Note1* | 0.3061 | 0.0941 | 7.0588 | 0.0954 | 0.0986 |
| *Note2* | 0.2896 | 0.0957 | 7.2707 | 0.1036 | 0.1153 |
| *PCB1* | 0.3069 | 0.0988 | 0.4513 | 0.1004 | 0.1283 |
| *PCB2* | 0.3361 | 0.1076 | 0.4779 | 0.1006 | 0.1319 |
| *Coin1* | 0.2954 | 0.0883 | 4.2589 | 0.1004 | 0.0992 |
| *Coin2* | 0.2771 | 0.0856 | 3.5649 | 0.0900 | 0.0912 |
| synchronization via trigger | | | | | |
| *Coin3* | 0.0686 | 0.0624 | 6.6274 | 0.0606 | 0.0617 |
| *No object* | 0.0612 | 0.0476 | - | 0.0481 | - |

tortions in our processed data increase. In this context, and as V1 BG and V2 BG and V2 FG achieve similar good results, V2 is typically the more practical choice. Figure 5 shows corresponding disparity maps for *Note1*, *PCB1*, *Coin1* and *Coin3*. The discussed reduction of artefacts (with V1 BG, V2 BG and V2 FG) and the failure case (V1 FG) are also evident in the visual examples.

We further observe (Table 1, Figure 5), that the largest improvements can be observed when applying our algorithm with disparities that were estimated from a background compared to a foreground stripe that might also contain a non-flat object. As our compensation approach strongly relies on its input disparities, we believe this observation also relates to their integrity. While the random color pattern in the background of our test data (e.g., Figure 5, views) typically eases the stereo matching process, textureless regions, repetitive patterns and glossy surfaces and occlusions might introduce erroneous disparities (Figure 5, c and d).

## Conclusion

Given a light field that was acquired with our setup, we were able to compensate for motion artefacts by leveraging the rich pixel information provided in the recorded light field. Our proposed approach, constrained the light field's transport position indices according the information obtained by comparing multiple views and enforcing uniform spacing between line acquisitions in a variational optimization procedure. Subsequently, the undistorted views were computed according to a warping function. To our knowledge, such a method did not exist before, especially for improving the integrity of light field data acquired in the line scan process. Performed evaluations demonstrated that our warping-based motion artefact compensation approach is able to significantly reduce (i.e., on average by a factor of 2.7) the mentioned motion artefacts in our test data, including acquisitions that were performed with a free running camera. A key advantage of the proposed approach, is that it allows multi-line scan light field imaging at virtually any magnification with correct resolution in the transport direction and in cases where the transport cannot be controlled with high precision.

## References


[1] Doris Antensteiner et al., High-Precision 3D Sensing with Hybrid Light Field & Photometric Stereo Approach in Multi-Line Scan Framework. Proceedings of IS&T Electronic Imaging 2017: Intelligent Robotics and Industrial Applications using Computer Vision, pp. 52-60. (2017).

[2] Robert Bolles et al., Epipolar-Plane Image Analysis: An Approach to Determining Structure from Motion. International Journal of Computer Vision, 1, 1 (1987).

[3] Roy Davies, Machine Vision: Theory, Algorithms, Practicalities. Morgan Kaufmann Publishers Inc., 2004.

[4] Bill Triggs et al., Bundle Adjustment - A Modern Synthesis, Proceedings of the International Workshop on Vision Algorithms 1999: Theory and Practice, pp. 298-372. (1999).

[5] Bernd Krolla, Maximilian Diebold and Didier Stricker, Light Field from Smartphone-Based Dual Video. Proceedings of European Conference on Computer Vision 2014, pp. 600-610. (2014).

[6] Gangjun Liu et al. Postprocessing Algorithms to Minimize Fixed-Pattern Artefact and Reduce Trigger Jitter in Swept Source Optical Coherence Tomography, Optics Express, 23, 8 (2015).

[7] Franz Pernkopf and Paul O'Leary, Image Acquisition Techniques for Automatic Visual Inspection of Metallic Surfaces, Non-destructive Testing & Enginieering, 36 (2003).

[8] Ariel Shamir and Olga Sorkine, Visual Media Retargeting, Proceedings of SIGGRAPH ASIA 2009 Courses, pg. 11. (2009).

[9] OpenCV, Open Source Computer Vision (2017).

[10] Svorad Štolc et al., Depth and All-in-Focus Imaging by a Multi-Line-Scan Light-Field Camera, Journal of Electronic Imaging, 23, 5 (2014).

[11] Thibaut Weise et al., Fast 3D Scanning with Automatic Motion Compensation, Proceedings of Conference on Computer Vision and Pattern Recognition 2007, pp. 1-8. (2007).

[12] Hang Yuet al., An Antivibration Time-Delay Integration CMOS Image Sensor With Online Deblurring Algorithm, Transactions on Circuits and Systems for Video Technology, 26, 8, 2016.


## Author Biography

*Dr. Nicole Brosch received her master's degree in Media Informatics (2009) and Computer Science Management (2010) from Vienna University of Technology. In 2016, she earned her PhD degree in Computer Science from Vienna University of Technology, where her main research focus was semi-automatic 2D-to-3D conversion of videos. In 2017 she joined AIT Austrian Institute of Technology GmbH (Vienna) as researcher at the Center for Vision, Automation & Control.*

*Dr. Svorad Štolc is a scientist in the Center for Vision, Automation & Control of the AIT Austrian Institute of Technology GmbH, Vienna. He graduated in Computer Science from Comenius University, Bratislava and earned his PhD degree in Bionics and Biomechanics from Technical University of Košice. He is (co)author of more than 50 peer-reviewed scientific papers and holds a number of patents in machine vision. Since 2016, he coordinates the computational imaging research activities at AIT with the focus on industrial inspection and document security.*

*Doris Antensteiner is a PhD candidate at the AIT Austrian Institute of Technology GmbH, (Vienna) in the field of computational imaging and computer vision. She received her master's degree with distinction at the Technical University of Vienna in 2011 in the field of computer science. After that she worked at Kapsch, Vienna at the R&D unit Vision and Sensor in the field of computer vision until she joined the AIT in 2015.*

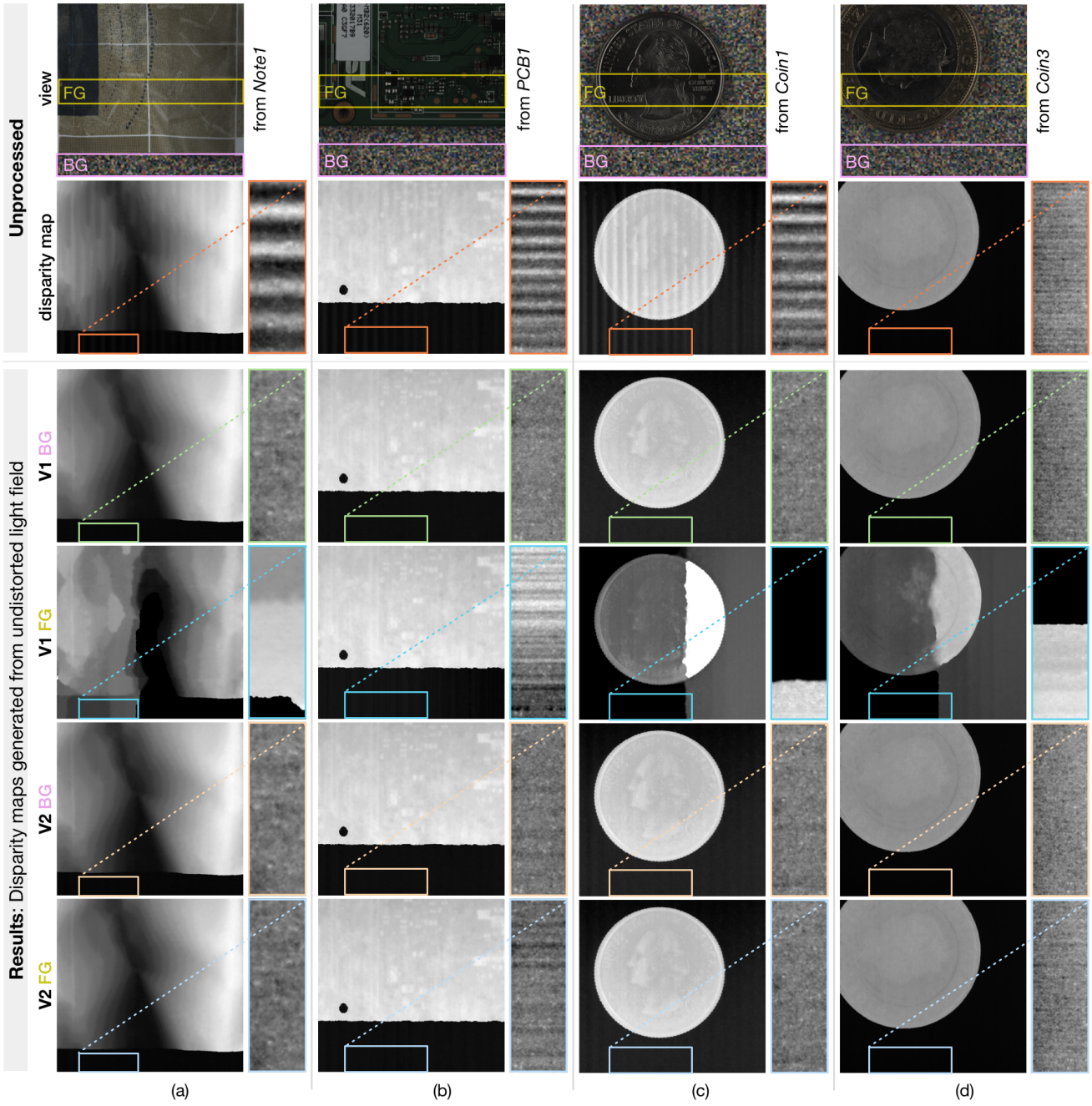


***Figure 5.*** *Visual comparisons of disparity maps generated from unprocessed distorted (top) and from our corrected (bottom) EPI stacks. Our approach was tested in two versions: with the first (V1) and the second version (V2) of our disparity term, and based on disparities that were estimated in background (BG) and foreground (FG) stripes of the distorted EPI stacks. The FG stripe (yellow) and BG stripe (pink) that were used in the disparity estimation are marked in the unprocessed views (top). The disparity maps shown as results were generated after undistorting the EPI stacks with our proposed approach. The motion artefacts are especially visible in the close-ups, which show intensity-normalized disparities of the marked regions in the disparity maps.*